Effects of Porosity and Amount of Surface Hydroxyl Groups of a Porous TiO2 Layer on the Performance of a CH3NH3PbI3 Perovskite Photovoltaic Cell

ARTICLE *in* THE JOURNAL OF PHYSICAL CHEMISTRY C · SEPTEMBER 2015

Impact Factor: 4.77 · DOI: 10.1021/acs.jpcc.5b05986

6 AUTHORS, INCLUDING:

Hasyiya Adli

Osaka University

8 PUBLICATIONS **22** CITATIONS

SEE PROFILE

Wilman Septina

University of Zurich

32 PUBLICATIONS **201** CITATIONS

SEE PROFILE

Seigo Ito

University of Hyogo

106 PUBLICATIONS **10,757** CITATIONS

SEE PROFILE

THE JOURNAL OF PHYSICAL CHEMISTRY C

Article

pubs.acs.org/JPCC

Effects of Porosity and Amount of Surface Hydroxyl Groups of a Porous TiO_2 Layer on the Performance of a $CH_3NH_3PbI_3$ Perovskite Photovoltaic Cell

Hasyiya Karimah Adli,[†] Takashi Harada,[†] Wilman Septina,[†] Shuji Hozan,[†] Seigo Ito,[‡] and Shigeru Ikeda*[,†]

[†]Research Center for Solar Energy Chemistry, Osaka University, 1-3 Machikaneyama, Toyonaka, Osaka 560-8531, Japan

[‡]Department of Electric Engineering and Computer Science, Graduate School of Engineering, University of Hyogo, 2167 Shosha, Himeji, Hyogo 671-2280, Japan

Supporting Information

ABSTRACT: The structural and physicochemcal properties of a porous titanium oxide layer (pTiO$_2$) in $CH_3NH_3PbI_3$ perovskite photovoltaic cells were systematically investigated by Raman spectroscopy, nitrogen sorption, and temperature desorption spectroscopy analyses. When the heat treatment temperature (T_{pTO}) during the fabrication of pTiO$_2$ was changed from 400 to 700 °C, its porosity and amount of surface hydroxyl groups were varied without alteration of the crystalline structure (anatase). Power conversion efficiencies (PCEs) of solar cells based on pTiO$_2$ prepared at different temperatures showed a volcanic-like pattern depending on T_{pTO} of pTiO$_2$; the highest PCE was obtained by using pTiO$_2$ prepared at T_{pTO} of 550 °C. Structural analyses of the $CH_3NH_3PbI_3$ perovskite part performed by X-ray diffraction indicated that formation of $CH_3NH_3PbI_3$ perovskite was inhibited by the presence of a large amount of surface hydroxyl groups on pTiO$_2$ prepared at relatively low T_{pTO} (<550 °C). On the other hand, significant reduction of porosity of pTiO$_2$ occurred when pTiO$_2$ was prepared at relatively high T_{pTO} (>550 °C) because of extinction of micropores and sintering between the TiO$_2$ particles; such a structural alteration hindered the penetration of CH_3NH_3I into the pore channel of TiO$_2$ filled by PbI_2, resulting in a large amount of PbI_2 remaining in the finally obtained photovoltaic cell. Hence, the optimum T_{pTO} (550 °C) for fabrication of pTiO$_2$ should be determined by its porous nature and sufficient removal of surface hydroxyl groups.

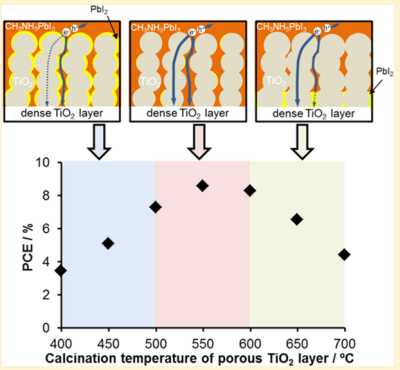

1. INTRODUCTION

Recently, organic−inorganic solar cells based on trihalide perovskites of the $CH_3NH_3PbX_3$ (X = I^-, Br^-, Cl^-) family have been gaining tremendous attention from scientific communities and commercial interests because of their cost effectiveness, ease of fabrication, and superb photovoltaic performances.[1−3] They are promising light absorbers for photovoltaics because of their advantages including suitable band gap energies for sunlight absorption (1.3−2.3 eV), high absorption coefficient (>10^4 cm^{-1}), and long-range exciton diffusion lengths (>1 μm).[4,5] Miyasaka et al. pioneered the work on a perovskite solar cell in 2009 with a power conversion efficiency (PCE) of 3.8% using an electrolyte as a hole-transporting material.[6] Subsequent improvement was achieved by optimizing the solution concentration, giving PCE of 6.54%.[7] Further studies resulted in incredible increases in the performance of perovskite solar cells with PCEs rising from 3.8% to 20.1% within five years.[8−17] Several different concepts applying unique properties of various organic−inorganic trihalide perovskites including thin-film planar heterojunctions,[18−21] heterojunctions with mesoporous metal oxide nanostructures,[22] and ordered nanotubes or nanowire metal oxides have been reported.[23−25]

Despite many reports of excellent PCEs, degradation of $CH_3NH_3PbX_3$ remains a severe obstacle for improvement of device performance. The effect of atmospheric moisture and humidity on $CH_3NH_3PbX_3$ is of interest because of its role in the degradation of solar cell performance.[26−28] In the presence of appreciable moisture, dark-brown $CH_3NH_3PbI_3$ compounds undergo rapid decomposition to yellowish lead(II) iodide (PbI_2), resulting in a significant decrease in PCE.[29,30] However, little is known about the degradation mechanism of the device upon exposure to moisture. Although a perovskite device can be prepared under ambient air, the degradation issue becomes a serious concern because of the normal high levels of humidity and moisture of ambient air. Snaith and co-workers reported that thermal stability and resistivity to moisture were improved by using P3HT/SWNTs-PMMA as a hole transport material (HTM).[29] Smith et al. also reported improvement of moisture stability by partial replacement of A-site cation ($CH_3NH_3^+$) with $C_6H_5(CH_2)_2NH_3^+$.[31]

Received: June 23, 2015
Revised: September 8, 2015

DOI: 10.1021/acs.jpcc.5b05986
J. Phys. Chem. C XXXX, XXX, XXX−XXX

Titanium oxide (TiO_2) is commonly used as a middle layer between perovskite and transparent conductive oxide (TCO) layers. It acts as an n-type semiconductor layer for accepting photoexcited electrons generated in the perovskite part analogous to dye-sensitized solar cells (DSSC).[32] The TiO_2 layer consists of two units: dense and porous units. The former is required for inhibiting shunting between TCO and HTM.[33] On the other hand, the latter acts as an electron transport material as well as a scaffold for efficient deposition of the perovskite layer from PbI_2 and CH_3NH_3I.[34] TiO_2 is also a typical photocatalyst with a band gap of 3.2 eV: this produces reactive oxygen species for water oxidation and oxidizing organic materials.[35] Thus, these TiO_2 components in perovskite solar cells would induce the device degradation. Indeed, Snaith et al. studied the stability of perovskite solar cells under UV radiation and suggested that oxygen (O_2) must be removed to suppress the degradation.[27] However, there have been few studies in which the effects of physical and chemical structures of TiO_2 on solar cell performance were investigated systematically.[34,36,37]

Recently, we found that the porosity and amount of surface hydroxyl (OH) groups of a porous TiO_2 layer ($p$$TiO_2$) are also important for effective conversion of perovskite in order to achieve better performance of solar cells. In this study, the effects of porosity and amount of OH groups in the $p$$TiO_2$ layer on the photovoltaic performance of resulting solar cells were investigated in relation to structures of $CH_3NH_3PbI_3$ perovskite.

2. EXPERIMENTAL SECTION

2.1. Fabrication of $CH_3NH_3PbI_3$ Perovskite Solar Cells. The $CH_3NH_3PbI_3$ perovskite solar cell was fabricated by following the reported procedure.[36] A fluorine-doped tin oxide (FTO)-coated glass substrate (FTO/glass, Nippon Sheet Glass, 9.7 Ω sq^{-1}) was cleaned with a detergent in an ultrasonic bath for 15 min and the rinsed with water and ethanol and exposed to the UV/O_3 for 15 min. A dense TiO_2 layer ($d$$TiO_2$) was deposited on the FTO/glass substrate by spray pyrolysis at 500 °C using 4 mL of ethanoic solution containing 0.3 mL of titanium diisoproxide bis(acetylacetonate) (TAA). Then the $p$$TiO_2$ layer was deposited on the $d$$TiO_2$-covered FTO/glass ($d$$TiO_2$/FTO/glass) by spin-coating of a commercial TiO_2 paste supplied by JGC Catalysts and Chemicals (PST-18NR) that was diluted with ethanol (TiO_2 paste:ethanol = 1:3.5) followed by heat treatment at various temperatures (400−700 °C) for 30 min. The $p$$TiO_2$ layers obtained by different calcination temperatures are denoted as $p$$TiO_2$(calcination temperature), e.g., $p$$TiO_2$ obtained by calcination at 400 °C is denoted as $p$$TiO_2$(400). PbI_2 dissolved in *N*,*N*-dimethylformamide (1.3 M) was spin-coated twice on the $p$$TiO_2$/$d$$TiO_2$/FTO/glass substrate, and the PbI_2-coated substrate was dried at 70 °C for 1 h. The resulting stacked film was then immersed in dehydrated isopropanol solution containing CH_3NH_3I (10 mg mL^{-1}),[34] followed by drying at 70 °C for 30 min. The process induced conversion of PbI_2 to $CH_3NH_3PbI_3$ perovskite. An HTM (i.e., Spiro-OMeTAD) was deposited on the $CH_3NH_3PbI_3$/$p$$TiO_2$/$d$$TiO_2$/FTO/glass stack by spin-coating using a chlorobenzene solution (0.06 M) containing lithium bis(trifluoromethane sulfonyl) imide (7 μL) and 4-*tert*-butylpyridine (11.5 μL). All of the above processes were conducted in open air with 30−50% humidity. Finally, an Au back contact was deposited by vacuum evaporation to obtain the perovskite solar cell with a structure of Au/HTM/$CH_3NH_3PbI_3$/$p$$TiO_2$/$d$$TiO_2$/FTO/glass.

2.2. Device Characterization. The crystalline structure of $p$$TiO_2$ was confirmed by Raman spectroscopy using a JASCO NRS-3100 laser Raman spectrophotometer with a laser wavelength of 532 nm. Specific surface area and porosity of $p$$TiO_2$ were analyzed by nitrogen (N_2) sorption at 77 K using a Quantachrome, AUTOSORB-1 automated gas sorption system. Thermal desorption spectroscopy (TDS) was conducted by using an ESCO HA1000PS instrument. Desorbed H_2O (m/z = 18) from the samples was detected by a standard quadrupole mass spectrometer when the temperature was increased from 50 to 550 °C at a heating ramp of 2 °C min^{-1}. Cross-sectional images of the films were observed by scanning electron microscopy using a Hitachi S-5000 field emission scanning electron microscopy (FE-SEM) instrument. Current density−voltage (J−V) characteristics of solar cells under simulated AM1.5G irradiation (100 mW cm^{-2}) were measured in the reverse direction (positive to negative) with a Bunkoh-Keiki CEP-015 photovoltaic measurement system. The cell area of the samples was 0.3 cm^2. Sheet resistance of the FTO substrate was measured by using a NAPSON RT-7 4-point probe resistivity measurement system. X-ray diffraction (XRD) patterns of samples were measured using a Rigaku MiniFlex X-ray diffractometer (Cu Kα, Ni filter).

3. RESULTS AND DISCUSSION

3.1. Characterizations of $p$$TiO_2$ Layers Calcined at Various Temperatures. Figure 1 shows Raman spectra of

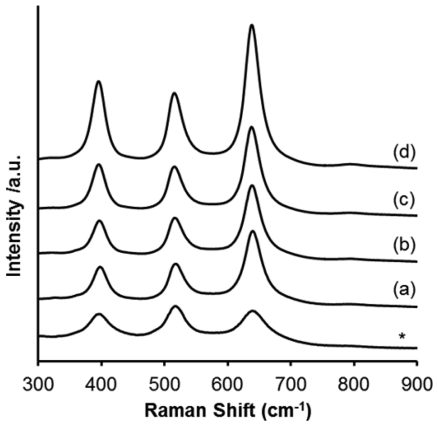

Figure 1. Raman spectra of $p$$TiO_2$ prepared at (a) 400 °C, (b) 500 °C, (c) 600 °C, and (d) 700 °C. Asterisk denotes the spectrum of commercial anatase TiO_2 powder.

$p$$TiO_2$ layers fabricated at various heat treatment temperatures (T_{pTO}s). A corresponding spectrum of commercial anatase TiO_2 powder is also shown for comparison. It is clear that all of the $p$$TiO_2$ layers showed characteristic peaks at 400, 520, and 641 cm^{-1}, corresponded to those of anatase TiO_2.[38] The TiO_2 paste used consisted of highly crystalline anatase; hence, we confirmed that the anatase crystalline structure was maintained even after heat treatment at 700 °C.

Figure 2 shows N_2 adsorption−desorption isotherms of $p$$TiO_2$ prepared at various T_{pTO} values. All of the isotherms showed a typical type IV isotherm according to the IUPAC nomenclature with a hysteresis loop. The presence of a hysteresis loop indicates that $p$$TiO_2$ samples have a pore structure with a mesoporous region between 2 and 50 nm.[39]

DOI: 10.1021/acs.jpcc.5b05986
J. Phys. Chem. C XXXX, XXX, XXX−XXX

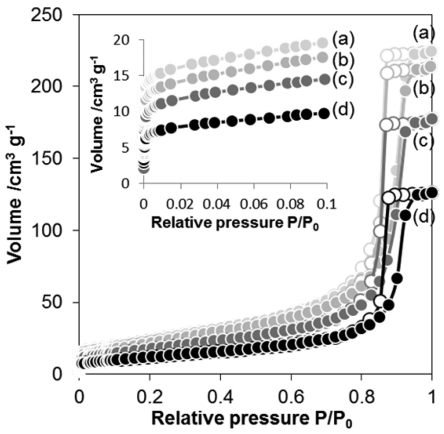

Figure 2. N_2 adsorption−desorption isotherms of pTiO$_2$ prepared at (a) 400 °C, (b) 500 °C, (c) 600 °C, and (d) 700 °C. Filled and open circles denote adsorption and desorption isotherms, respectively.

Moreover, observations of steep increases at a low relative pressure region (p/p_0 < 0.1) indicate the presence of a micropore (<2 nm) system. By analysis of the adsorption branch of an isotherm by the BJH method, mesopore size distributions (W_{meso}) of pTiO$_2$ were determined.[39] The volumes of mesopores (V_{meso}) and micropores (V_{micro}) of pTiO$_2$ were also determined by the t-plot method. Table 1

Table 1. Structural Parameters of Various pTiO$_2$ Samples Obtained by N_2 Sorption Measurements

T_{pTO}[a] (°C)	W_{meso}[b] (nm)	V_{meso}[c] (cm^3 g^{-1})	V_{micro}[d] (cm^3 g^{-1})	S_{BET}[e] (m^2 g^{-1})
400	24	0.34	0.0079	84
450	24	0.32	0.0073	81
500	24	0.32	0.0065	83
550	24	0.29	0.0067	80
600	24	0.26	0.0047	66
650	24	0.22	0.0043	55
700	23	0.17	0.0035	41

[a]Heat treatment temperature. [b]Average mesopore size. [c]Mesopore volume. [d]Micropore volume. [e]Specific surface area.

summarizes the results together with corresponding specific surface areas determined by the BET method (S_{BET}). Although W_{meso} values were almost constant (see Figure S1), V_{meso} values decreased gradually with increase in heat treatment temperature over 550 °C during the fabrication of pTiO$_2$. A similar trend, i.e., a steady decrease with increase in the heat treatment temperature, was also obtained for S_{BET} and V_{micro} values, suggesting gradual extinction of mesopore and micropore channels induced by relatively high-temperature heat treatment during fabrication of pTiO$_2$. Significant decreases of S_{BET}, V_{meso}, and V_{micro} of temperatures over 550 °C are likely to be induced by sintering of TiO$_2$ particles. Such growth of TiO$_2$ particles was also indicated by corresponding cross-sectional SEM images, as shown in Figure S2: the size of TiO$_2$ particles became appreciably larger when the sample was fabricated at a temperature higher than 650 °C.

Figure 3 shows TDS spectra (m/z = 18) of pTiO$_2$ fabricated at various T_{pTO}s. The pTiO$_2$(400) sample showed a distinct peak in the region of 50−100 °C and a broad tail in the region of 100−450 °C. The former was attributed to physisorbed water and the latter was derived from the surface OH groups. It

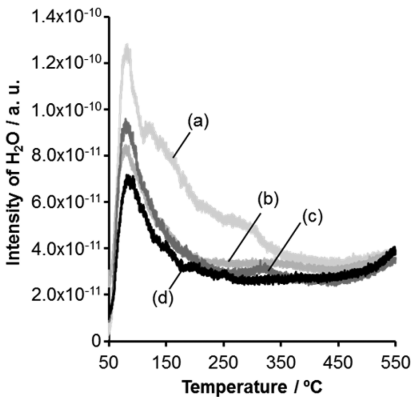

Figure 3. TDS spectra of pTiO$_2$ prepared at (a) 400 °C, (b) 500 °C, (c) 600 °C, and (d) 700 °C.

is clear from the figure that the amounts of both physisorbed water and surface OH groups decreased with increase in T_{pTO} during fabrication of pTiO$_2$. Because the decrease of surface OH groups should result in a decrease in surface hydrophilicity, the observed relationship between amounts of physisorbed water and surface OH groups is reasonable.[40]

3.2. Performance of $CH_3NH_3PbI_3$ Perovskite Solar Cells and Characterization of the $CH_3NH_3PbI_3$ Layers Deposited on Porous TiO$_2$ Layers Heated at Various Temperatures. Photovoltaic properties of devices containing pTiO$_2$ prepared at various heat treatment temperatures were evaluated under simulated sunlight (AM1.5G) irradiation. In this study, the $CH_3NH_3PbI_3$ perovskite was deposited by the so-called two-step method involving deposition of PbI_2 and subsequent reaction with CH_3NH_3I (see Experimental Section) because this is one of the most reproducible methods for obtaining active solar cells with good PCEs.[14] For each device containing pTiO$_2$ obtained at the same temperature, we made six samples to confirm reproducibility of device properties. As shown in Figure 4, thus-obtained device parameters, i.e., short circuit current density (J_{SC}), open circuit voltage (V_{OC}), fill factor (FF), and PCE, were plotted as a function of heat treatment temperature during the fabrication of pTiO$_2$. The J_{SC} value showed appreciable dependence on the kind of pTiO$_2$

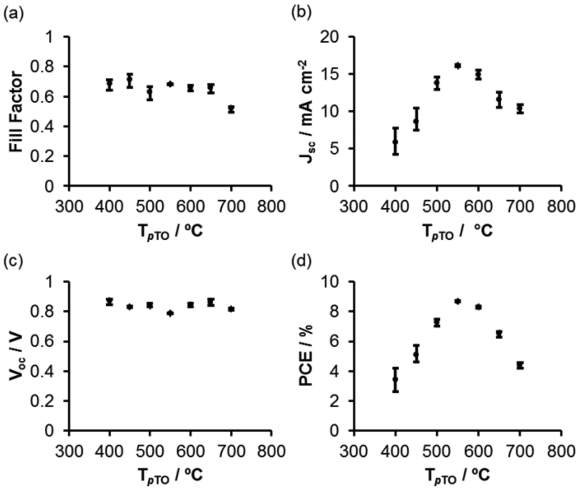

Figure 4. (a) Fill factors, (b) J_{SC} values, (c) V_{oc} values, and (d) PCEs of $CH_3NH_3PbI_3$ perovskite solar cells composed of pTiO$_2$ prepared at various temperatures.

DOI: 10.1021/acs.jpcc.5b05986
J. Phys. Chem. C XXXX, XXX, XXX−XXX

used: the value gradually increased with increase in preparation temperature of pTiO$_2$ at around 550−600 °C and decreased again when pTiO$_2$ samples prepared at higher heat treatment temperatures were used. On the other hand, both V_{OC} and FF values showed no dependence on the pTiO$_2$ used with the exception of the FF value for the cell composed of pTiO$_2$(700). In a separate experiment, sheet resistances (R_s) of FTO/glass after heat treatment at various temperatures were measured. As shown in Figure S3, the R_s value of the FTO/glass after heating at 700 °C was appreciably large compared to the values for FTO/glass samples with relatively low-temperature heat treatments. Thus, the observed drop of FF in the cell composed of pTiO$_2$(700) was likely to be derived from the increment of R_s of FTO/glass. In regard to the PCE values, a volcano-type temperature dependence was clearly observed, similar to the trend observed for J_{SC}. One of the devices composed of pTiO$_2$(550) showed the highest PCE of 8.8% in the series of the present devices. The cross-sectional SEM image of this solar cell is shown in Figure S2.

Structural analyses of the devices were performed by XRD to determine the dependences of J_{SC} and that of PCE on the kind of pTiO$_2$ used. Figure 5 shows typical results obtained for

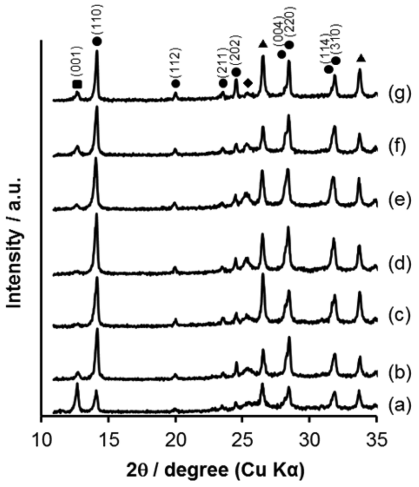

Figure 5. XRD patterns of $CH_3NH_3PbI_3$ perovskite films deposited on pTiO$_2$ layers prepared at (a) 400 °C, (b) 450 °C, (c) 500 °C, (d) 550 °C, (e) 600 °C, (f) 650 °C, and (g) 700 °C. The square, circle, rhombus, and triangle symbols denote reflections assignable to PbI_2, $CH_3NH_3PbI_3$, TiO$_2$, and FTO, respectively.

devices composed of pTiO$_2$ prepared at different heat treatment temperatures in a limited 2θ range (10°−35°). In addition to strong reflections derived from FTO, various reflection peaks were observed. Most of the reflections were derived from those of tetragonal $CH_3NH_3PbI_3$ perovskite[41,42] with the exception of the reflection at 2θ of 12.7°, which could be assigned to the (001) plane of PbI_2. Because (001) reflection of PbI_2 was observed in all of the samples, complete conversion of PbI_2 to $CH_3NH_3PbI_3$ perovskite did not proceed. Therefore, for evaluation of the relative contents of $CH_3NH_3PbI_3$ perovskite and PbI_2, a peak intensity ratio of $CH_3NH_3PbI_3$ (110) to PbI_2 (001) (perov/iodide) was introduced, and thus-obtained values were plotted as a function of heat treatment temperatures during preparation of pTiO$_2$ (Figure 6). Clearly, the perov/iodide values showed a volcanic-like pattern similar to that observed for J_{SC} and PCEs (see Figure 4b,d).

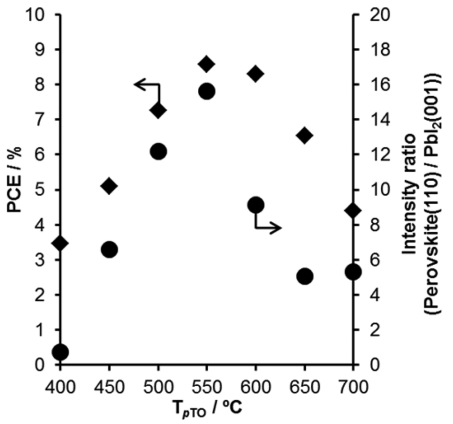

Figure 6. Plots of PCEs (diamonds) and perov/iodide values of $CH_3NH_3PbI_3$ perovskite layers (circles) as a function of preparation temperatures of pTiO$_2$.

Based on the above results, schematic illustrations of structures of pTiO$_2$−$CH_3NH_3PbI_3$ perovskite junctions formed by using various pTiO$_2$s are shown in Figure 7. As discussed above, pTiO$_2$ prepared at relatively low heat treatment temperatures included large amounts of surface OH groups, thus leading to an increase in physisorbed H_2O. The weakness of $CH_3NH_3PbI_3$ perovskites toward moisture is widely known, and several reports discussed decomposition pathway(s) of $CH_3NH_3PbI_3$ in the presence of water.[43,44] In the present system, therefore, as-formed $CH_3NH_3PbI_3$ perovskites at the interface of TiO$_2$ surface decomposed intensively because of the presence of physisorbed water on the TiO$_2$ surface. The PbI_2 component blocks the electron transfer from the $CH_3NH_3PbI_3$ to TiO$_2$ because the conduction band of PbI_2 (−3.45 eV below vacuum level) is higher than that of $CH_3NH_3PbI_3$ (−3.93 eV below vacuum level).[45] Therefore, appreciable reductions of J_{SC} values accompanied by decrease in PCEs were observed, as shown in Figure 7a. The achievement of both large J_{SC} values and large PCEs obtained for the cells based on pTiO$_2$(550) and pTiO$_2$(600) can also be explained by this hypothesis because these devices should include relatively small amounts of PbI_2 at the surface of pTiO$_2$ (Figure 7b). When the calcination temperature was increased over 600 °C, significant reduction of porosity occurred. Especially, decrease in the V_{meso} value significantly affected the pore system because V_{meso} values are different by 2 orders of magnitude from V_{micro} values. In this situation, diffusion of CH_3NH_3I into pTiO$_2$ filled with PbI_2 was inhibited: this resulted in increment of unreacted PbI_2 specifically at the bottom part of pTiO$_2$ (Figure 7c). The PbI_2 layer also suppressed electron transfer from $CH_3NH_3PbI_3$ to dTiO$_2$, inducing a decrease in J_{SC} values and thus a decrease in PCEs.

4. CONCLUSION

In this study, the dependence of photovoltaic properties of $CH_3NH_3PbI_3$ perovskite solar cells on structural and physicochemical properties of pTiO$_2$ was examined. As a result, the optimum pTiO$_2$ was found to have two important properties: small amount of surface OH groups and a sufficiently developed pore system. The former would be difficult to achieve by using usual pTiO$_2$ prepared at relatively low temperatures, whereas the latter can be achieved by using such a low-temperature processed pTiO$_2$. Therefore, for the development of a low-temperature process to reduce and/or

DOI: 10.1021/acs.jpcc.5b05986
J. Phys. Chem. C XXXX, XXX, XXX−XXX

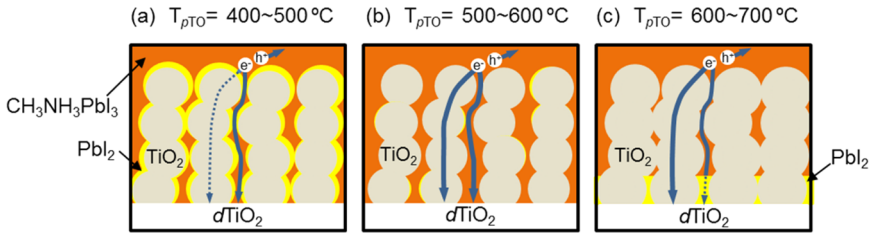

Figure 7. Schematic illustrations of $CH_3NH_3PbI_3$ perovskite-pTiO$_2$ junctions formed by using pTiO$_2$ prepared at relatively (a) low, (b) moderate, and (c) high temperatures.

simplify the production scheme of a $CH_3NH_3PbI_3$ perovskite solar cell, there should be effective treatments to reduce surface OH groups in low-temperature-processed pTiO$_2$. Study along this line is now in progress.

■ ASSOCIATED CONTENT

Supporting Information

The Supporting Information is available free of charge on the ACS Publications website at DOI: 10.1021/acs.jpcc.5b05986.

BJH plots and cross-sectional SEM images of pTiO$_2$ prepared at various temperatures, cross-sectional SEM image of $CH_3NH_3PbI_3$ perovskite solar cell, and a plot of the resistivity of FTO as a function of heat treatment temperature (PDF)

■ AUTHOR INFORMATION

Corresponding Author

*E-mail: sikeda@chem.es.osaka-u.ac.jp. Tel: +81-6-6850-6696. Fax: +81-6-6850-6699.

Notes

The authors declare no competing financial interest.

■ ACKNOWLEDGMENTS

This work was supported by a Grant-in-Aid for Scientific Research on Innovative Areas (All Nippon Artificial Photosynthesis Project for Living Earth), a Grant-in-Aid for Scientific Research (B), and a Grant-in-Aid for Challenging Exploratory Research from MEXT Japan. One of the authors (H.K.A.) thanks Ministry of Education (Malaysia) and University Malaysia Kelantan for providing a scholarship during the study.

■ REFERENCES

(1) Hodes, G. Perovskite-Based Solar Cells. *Science* **2013**, *342*, 317−318.
(2) Snaith, H. J. Perovskites: the Emergence of a New Era for Low-Cost, High-Efficiency Solar Cells. *J. Phys. Chem. Lett.* **2013**, *4*, 3623−3630.
(3) Park, N.-G. Organometal Perovskite Light Absorbers Toward a 20% Efficiency Low-Cost Solid-State Mesoscopic Solar Cell. *J. Phys. Chem. Lett.* **2013**, *4*, 2423−2429.
(4) Stranks, S. D.; Eperon, G. E.; Grancini, G.; Menelaou, C.; Alcocer, M. J. P.; Leijtens, T.; Herz, L. M.; Petrozza, A.; Snaith, H. J. Electron-Hole Diffusion Lengths Exceeding 1 Micrometer in an Organometal Trihalide Perovskite Absorber. *Science* **2013**, *342*, 341−344.
(5) Xing, G.; Mathews, N.; Sun, S.; Lim, Y. M.; Lam, Y. M.; Grätzel, M.; Mhaisalkar, S.; Sum, T. C. Long-Range Balanced Electron and Hole-Transport Lengths in Organic-Inorganic $CH_3NH_3PbI_3$. *Science* **2013**, *342*, 344−347.
(6) Kojima, A.; Teshima, K.; Shirai, Y.; Miyasaka, T. Organometal Halide Perovskites as Visible-Light Sensitizers for Photovoltaic Cells. *J. Am. Chem. Soc.* **2009**, *131*, 6050−6051.
(7) Im, J. H.; Lee, C. R.; Lee, J. W.; Park, S. W.; Park, N. G. 6.5% Efficient Perovskite Quantum-Dot-Sensitized Solar Cell. *Nanoscale* **2011**, *3*, 4088−4093.
(8) National Renewable Energy Laboratory. Best Research-Cell Efficiencies. http://www.nrel.gov/ncpv/images/efficiency_chart.jpg (accesed May 19, 2015).
(9) Wojciechowski, K.; Saliba, M.; Leijtens, T.; Abate, A.; Snaith, H. J. Sub 150 °C Processed Meso-Superstructured Perovskite Solar Cells with Enhanced Efficiency. *Energy Environ. Sci.* **2014**, *7*, 1142−1147.
(10) Wang, Q.; Shao, Y. C.; Dong, Q. F.; Xiao, Z. G.; Yuan, Y. B.; Huang, J. S. Large Fill-Factor Bilayer Iodine Perovskite Solar Cells Fabricated by a Low-Temperature Solution-Process. *Energy Environ. Sci.* **2014**, *7*, 2359−2365.
(11) Jeon, N. J.; Lee, H. G.; Kim, Y. C.; Seo, J.; Noh, J. H.; Lee, J.; Seok, S. I. o-Methoxy Substituents in Spiro-OMetad for Efficient Inorganic-Organic Hybrid Perovskite Solar Cells. *J. Am. Chem. Soc.* **2014**, *136*, 7837−7840.
(12) Ryu, S.; Noh, J. H.; Jeon, N. J.; Kim, Y. C.; Yang, S.; Seo, J. W.; Seok, S. I. Voltage Output of Efficient Perovskite Solar Cells with High Open-Circuit Voltage and Fill Factor. *Energy Environ. Sci.* **2014**, *7*, 2614−2618.
(13) Liu, M. Z.; Johnston, M. B.; Snaith, H. J. Efficient Planar Heterojunction Perovskite Solar Cells by Vapour Deposition. *Nature* **2013**, *501*, 395−398.
(14) Burschka, J.; Pellet, N.; Moon, S. J.; Humphry-Baker, R.; Gao, P.; Nazeeruddin, M. K.; Gratzel, M. Sequential Deposition as a Route to High-Performance Perovskite-Sensitized Solar Cells. *Nature* **2013**, *499*, 316−319.
(15) Jeon, N. J.; Noh, J. H.; Kim, Y. C.; Yang, W. S.; Ryu, S.; Seok, S. I. Solvent Engineering for High-Performance Inorganic- Organic Hybrid Perovskite Solar Cells. *Nat. Mater.* **2014**, *13*, 897−903.
(16) Zhou, H. P.; Chen, Q.; Li, G.; Luo, S.; Song, T. B.; Duan, H. S.; Hong, Z. R.; You, J. B.; Liu, Y. S.; Yang, Y. Interface Engineering of Highly Efficient Perovskite Solar Cells. *Science* **2014**, *345*, 542−546.
(17) Green, M. A.; Emery, K.; Hishikawa, Y.; Warta, W.; Dunlop, E. D. Solar Cell Efficiency Tables (Version 44). *Prog. Photovoltaics* **2014**, *22*, 701−710.
(18) Conings, B.; Baeten, L.; De Dobbelaere, C.; D'Haen, J.; Manca, J.; Boyen, H.-G. Perovskite-Based Hybrid Solar Cells Exceeding 10% Efficiency with High Reproducibility Using a Thin Film Sandwich. *Adv. Mater.* **2014**, *26*, 2041−2046.
(19) Docampo, P.; Ball, J. M.; Darwich, M.; Eperon, G. E.; Snaith, H. J. Efficient Organometal Trihalide Perovskite Planar-Heterojunction Solar Cells on Flexible Polymer Substrates. *Nat. Commun.* **2013**, *4*, 2761−2767.
(20) Eperon, G. E.; Burlakov, V. M.; Docampo, P.; Goriely, A.; Snaith, H. J. Morphological Control for High Performance, Solution-Processed Planar Heterojunction Perovskite Solar Cells. *Adv. Funct. Mater.* **2014**, *24*, 151−157.
(21) Liu, M.; Johnston, M. B.; Snaith, H. J. Efficient Planar Heterojunction Perovskite Solar Cells by Vapour Deposition. *Nature* **2013**, *501*, 395−398.
(22) You, J.; Hong, Z.; Yang, Y. M.; Chen, Q.; Cai, M.; Song, T. B.; Chen, C. C.; Lu, S.; Liu, Y.; Zhou, H.; et al. Low-Temperature Solution-Processed Perovskite Solar Cells with High Efficiency and Flexibility. *ACS Nano* **2014**, *8*, 1674−1680.

DOI: 10.1021/acs.jpcc.5b05986
J. Phys. Chem. C XXXX, XXX, XXX−XXX

(23) Edri, E.; Kirmayer, S.; Henning, A.; Mukhopadhyay, S.; Gartsman, K.; Rosenwaks, Y.; Hodes, G.; Cahen, D. Why Lead Methylammonium Tri-Iodide Perovskite-Based Solar Cells Require a Mesoporous Electron Transporting Scaffold (but Not Necessarily a Hole Conductor). *Nano Lett.* **2014**, *14*, 1000−1004.
(24) Kim, H.-S.; Lee, J. W.; Yantara, N.; Boix, P. P.; Kulkarni, S. A.; Mhaisalkar, S.; Grätzel, M.; Park, N.-G. High Efficiency Solid-State Sensitized Solar Cell-Based on Submicrometer Rutile TiO_2 Nanorod and $CH_3NH_3PbI_3$ Perovskite Sensitizer. *Nano Lett.* **2013**, *13*, 2412−2417.
(25) Kumar, M. H.; Yantara, N.; Dharani, S.; Grätzel, M.; Mhaisalkar, S.; Boix, P. P.; Mathews, N. Flexible, Low-Temperature, Solution Processed ZnO-Based Perovskite Solid State Solar Cells. *Chem. Commun.* **2013**, *49*, 11089−11091.
(26) Bass, K. K.; McAnally, R. E.; Zhou, S.; Djurovich, P. I.; Thompson, M. E.; Melot, B. C. Influence of Moisture on the Preparation, Crystal Structure, and Photophysical Properties of Organohalide Perovskites. *Chem. Commun.* **2014**, *50*, 15819−15822.
(27) Leijtens, T.; Eperon, G. E.; Pathak, S.; Abate, A.; Lee, M. M.; Snaith, H. J. Overcoming Ultraviolet Light Instability of Sensitized TiO_2 with Meso-Superstructured Organometal Tri-Halide Perovskite Solar Cells. *Nat. Commun.* **2013**, *4*, 2885.
(28) Noh, J. H.; Im, S. H.; Heo, J. H.; Mandal, T. N.; Seok, S. Il. Chemical Management for Colorful, Efficient, and Stable Inorganic-Organic Hybrid Nanostructured Solar Cells. *Nano Lett.* **2013**, *13*, 1764−1769.
(29) Habisreutinger, S. N.; Leijtens, T.; Eperon, G. E.; Stranks, S. D.; Nicholas, R. J.; Snaith, H. J. Carbon Nanotube/Polymer Composites as a Highly Stable Hole Collection Layer in Perovskite Solar Cells. *Nano Lett.* **2014**, *14*, 5561−5568.
(30) Christians, J. A.; Herrera, P. A. M.; Kamat, P. V. Transformation of the Excited State and Photovoltaic Efficiency of $CH_3NH_3PbI_3$ Perovskite upon Controlled Exposure to Humidified Air. *J. Am. Chem. Soc.* **2015**, *137*, 1530−1538.
(31) Smith, I. C.; Hoke, E. T.; Solis-Ibarra, D.; McGehee, M. D.; Karunadasa, H. I. A Layered Hybrid Perovskite Solar-Cell Absorber with Enhanced Moisture Stability. *Angew. Chem.* **2014**, *126*, 11414−11417.
(32) Qiu, J.; Qiu, Y.; Yan, K.; Zhong, M.; Mu, C.; Yan, H.; Yang, S. All-Solid-State Hybrid Solar Cells Based on a New Organometal Halide Perovskite Sensitizer and One-Dimensional TiO_2 Nanowire Arrays. *Nanoscale* **2013**, *5*, 3245−3248.
(33) Wang, X.; Fang, Y.; He, L.; Wang, Q.; Wu, T. Influence of Compact TiO_2 Layer on the Photovoltaic Characteristics of the Organometalhalide Perovskite-Based Solar Cells. *Mater. Sci. Semicond. Process.* **2014**, *27*, 569−576.
(34) Etgar, L.; Gao, P.; Xue, Z.; Peng, Q.; Chandiran, A. K.; Liu, B.; Nazeeruddin, M. K.; Grätzel, M. Mesoscopic $CH_3NH_3PbI_3/TiO_2$ Heterojunction Solar Cell. *J. Am. Chem. Soc.* **2012**, *134*, 17396−17399.
(35) Fujishima, A.; Rao, T. N.; Tryk, D. A. Titanium Dioxide Photocatalysis. *J. Photochem. Photobiol., C* **2000**, *1*, 1.
(36) Murugadoss, G.; Mizuta, G.; Tanaka, S.; Nishino, H.; Umeyama, T.; Imahori, H.; Ito, S. Double Functions of Porous TiO_2 Electrodes on $CH_3NH_3PbI_3$ Perovskite Solar Cells: Enhancement of Perovskite Crystal Transformation and Prohibition of Short Circuiting. *APL Mater.* **2014**, *2*, 081511-1−081511-6.
(37) Dharani, S.; Mulmudi, H. K.; Yantara, N.; Thu Trang, P. T.; Thi, P.; Park, N.-G.; Grätzel, M.; Mhaisalkar, S.; Mathews, N.; Boix, P. P. High Efficiency Electrospun TiO_2 Nanofiber Based Hybrid Organic-Inorganic Perovskite Solar Cell. *Nanoscale* **2014**, *6*, 1675−1679.
(38) Lee, J.-W.; Lee, T.-Y.; Yoo, P. J.; Grätzel, M.; Mhaisalkar, S.; Park, N.-G. Rutile TiO_2-Based Perovskite Solar Cells. *J. Mater. Chem. A* **2014**, *2*, 9251−9259.
(39) Kaneko, K. Determination of Pore Size and Pore Size Distribution: 1. Adsorbents and Catalysts. *J. Membr. Sci.* **1994**, *96*, 59−89.
(40) Liu, L.-M.; Crawford, P.; Hu, P. The Interaction Between Adsorbed OH and O_2 on TiO_2 Surfaces. *Prog. Surf. Sci.* **2009**, *84*, 155−176.
(41) Baikie, T.; Fang, Y.; Kadro, J. M.; Schreyer, M.; Wei, F.; Mhaisalkar, S. G.; Gratzel, M.; White, T. J. Synthesis and Crystal Chemistry of the Hybrid Perovskite $(CH_3NH_3)PbI_3$ for Solid-State Sensitised Solar Cell Applications. *J. Mater. Chem. A* **2013**, *1*, 5628−5641.
(42) Ogomi, Y.; Morita, A.; Tsukamoto, S.; Saitho, T.; Shen, Q.; Toyoda, T.; Yoshino, K.; Pandey, S. S.; Ma, T.; Hayase, S. All-Solid Perovskite Solar Cells with HOCO-R-$NH_3^+I^-$ Anchor-Group Inserted between Porous Titania and Perovskite. *J. Phys. Chem. C* **2014**, *118*, 16651−16659.
(43) Han, Y.; Meyer, S.; Dkhissi, Y.; Weber, Ka; Pringle, J. M.; Bach, U.; Spiccia, L.; Cheng, Y.-B. Degradation Observations of Encapsulated Planar $CH_3NH_3PbI_3$ Perovskite Solar Cells at High Temperatures and Humidity. *J. Mater. Chem. A* **2015**, *3*, 8139−8147.
(44) Mosconi, E.; Azpiroz, J. M.; De Angelis, F. Ab Initio Molecular Dynamics Simulations of Methylammonium Lead Iodide Perovskite Degradation by Water. *Chem. Mater.* **2015**, *27*, 4885−4892.
(45) Chen, Q.; Zhou, H.; Song, T.-B.; Luo, S.; Hong, Z.; Duan, H.-S.; Dou, L.; Liu, Y.; Yang, Y. Controllable Self-Induced Passivation of Hybrid Lead Iodide Perovskites toward High Performance Solar Cells. *Nano Lett.* **2014**, *14*, 4158−4163.

DOI: 10.1021/acs.jpcc.5b05986
J. Phys. Chem. C XXXX, XXX, XXX−XXX